exeley INTERNATIONAL JOURNAL ON SMART SENSING AND INTELLIGENT SYSTEMS

Article | DOI: 10.21307/ijssis-2019-012

Issue 1 | Vol. 13 (2020)

Modeling and experimental validation of the hysteretic dynamics of shape memory alloy springs

R. A. Abubakar, Yutian Hu, Fan Wang and Linxiang Wang

The State Key Laboratory for Fluid Power and Mechatronic Systems, Zhejiang University, 310027, Hangzhou, China.

E-mails: rbkiru@yahoo.com, huyutian213@163.com, 11725076@zju.edu.cn, wanglx236@zju.edu.cn

The paper was edited by Md. Eshrat E. Alahi.

Received for publication November 23, 2019.

Abstract

In this work, the hysteretic dynamics of a pseudoelastic shape memory alloy (SMA) spring is modeled and tested. A constitutive model of SMA spring is constructed by combining the theory of mechanical spring and the derived SMA constitutive relation. The SMA spring recovery force is modeled by employing the Euler–Lagrange equation based on a non-convex potential function. A macroscopic differential model is formulated to describe the hysteretic dynamics and the pseudoelasticity of the SMA spring. A theoretical method for estimating the equivalent stretch ratio at a specific temperature of SMA spring is given. Numerical simulations were presented in studying the influence of the stretch ratio at a temperature of 50, 70, and 90°C. The experimental tests are performed and presented together with their numerical counterparts. The comparison is made between numerical and experimental results to validate the proposed model for SMA spring.

Keywords

Shape memory alloys spring, Martensitic transformation, Pseudoelasticity, Differential model.

Shape memory alloys (SMA) are special alloys developed with the special property that when it is deformed, by increasing temperature it regains back to its initial shape. Even under high applied load, the increasing temperature can result in actuation (Kumar and Lagoudas, 2008). Though they exhibit a low-frequency response, SMAs exhibit a reversible hysteresis property under mechanical cyclic loading (Rao et al., 2015). This makes them an essential material in many engineering applications such as actuation impact absorption (Pirbhulal et al., 2017), sensor (Alahi et al., 2018; Pirbhulal, 2019), and vibration isolation to mention some. With the exception of the medical field, such as wearable devices, IoT, tele-healthcare (Wu et al., 2018), SMAs have not been commercialized due to the lack of a detailed model that describes their behaviors. For the past two decades, many mathematical models have been constructed for SMA from different perspectives (Pirbhulal et al., 2017; Alahi et al., 2018). However, due to the complex behavior of SMA, an exact and simple model has not yet been developed. Recently, SMA spring has attracted researchers' attention due to its outstanding features in the field of actuators and vibration control. As an actuator, an SMA spring results in a much larger displacement than SMA wire. When SMA wire is formed as spring, it also enlightens the existing vibration isolation solution for its internal damping capability and pseudoelasticity. However, the pursuit of modeling its dynamic process is still under the spotlight.

Claire Morin et al. (2011) introduced a model with the name Zaki–Moumni (ZM) model. Here stain rate induced by the mechanical pseudoelasticity is considered, but the achievement is only at a high strain rate probably due to localization effect. Wang et al. (2017) developed a constitute model for simulation of SMA Nitinol at different loading rates. The model

is described by cyclic pseudoelasticity of polycrystalline SMAs. But the constitute model equations are not easy to execute. Other methods have been employed to verify the model cyclic capability in a multi-axial problem.

Compared to SMA wire and bar, SMA spring has a larger actuation stroke which qualifies it for many engineering applications. In designing SMA spring, the stiffness, actuating force, length, and applied force direction are usually determined by the dimensions like wire diameter, spring diameter, number of coil, and pitch angle (Liang and Rogers, 1990; Wu et al., 2018). Because of the complex thermo-mechanical behavior of SMA springs, it is difficult to make an exact and simpler model that can solve its thermo-mechanical behavior. This also limits their engineering applications. Some efforts have been made to model the thermo-mechanical behavior. C. Liang first explores the applications of SMA spring in vibration control (Liang and Rogers, 1993). Based on the constitutive relations of nonlinear thermo-mechanical SMA, the corresponding method for designing SMA spring was introduced. But the model was not validated with experiment values to determine its accuracy. Gédouin et al. (2019) proposed a model in which de-twinning and two-way memory effects are modeled based on the theory of R-phase of helical SMA spring to get thermo-mechanical actuation. The model is restricted to only R-phase transformation. Toi et al. presented their model using the finite element method and Timoshenko beam formula by the approach of the Lagrangian super-elastic deformation of SMA spring under compression and tension (Enemark et al., 2016). However, torsional deformation is not considered which is also very important in determining the deformation of an element (Toi et al., 2004). Tobushi and Kikuaki (1991) introduce a model for the deformation of SMA spring under compression. But the model could not be applied for the tensile test, which is easy to perform as the material test on the wire. To establish the methods which are possible to apply directly for the design of the helical spring, and to construct deformation equations considering the cyclic deformation properties of the helical spring, Dong et al. applied a finite element method to develop an SMA spring model (Dong et al., 2008). In its experimental form, the changeable airfoil is actuated by SMA spring. However, the stress and strain distribution cross-section were complex.

Inspired by the above recent attempts, the proposal and novelty of this work are to construct an appropriate and simpler model for SMA spring that can capture better the pseudoelasticity precisely than the existent models mentioned above. In many engineering applications of SMA spring, it is also desired that the SMA spring model should be easy to be analyzed and controlled. In this work, a Landau-type torsional free energy is established based on Ginzburg–Landau theory which is capable of describing phase transformation. A phenomenological model for SMA spring is proposed and experiments tests are conducted to get experimental data. The proposed model is formulated as a second-order ordinary differential equation, which is very convenient for system dynamic analysis and implementing of modern control technology. A comparison between experimental and model data presents an approximate agreement.

Constitution relationship of SMA wire

In the Lagrangian mechanics, the following equation could be taken as the Lagrangian of the SMA rod which consists of ki. and potential energy in mechanical fields (Zhou and Feng, 2009):

$$L = \int \left(\frac{\rho}{2} (\dot{u})^2 - F \right) dx, \tag{1}$$

where ρ, u, and F stand for density, displacement, and potential energy function, respectively, while $\frac{\rho}{2}(\dot{u})^2$ is the kinetic energy density. The essence of Ginzburg–Landau theory for modeling of phase transition is that the involved potential energy density function is a non-convex function of the order parameter and temperature θ. Here the strain $\varepsilon(x, t) = \partial u/\partial x$ is chosen order parameter, and the potential energy density is constructed as Landau free energy function $F_1(\theta, \varepsilon)$, which is taken as the same form as established earlier (Bales and Gooding, 1991; Wang and Melnik, 2004; Wang and Melnik, 2012):

$$F_1(\theta, \varepsilon) = \frac{k_1(\theta - \theta_c)}{2} \varepsilon^2 + \frac{k_2}{4} \varepsilon^4 + \frac{k_3}{6} \varepsilon^6, \tag{2}$$

where θ is the material temperature; k_1, k_2, and k_3 are material constants; and θ_c is the critical temperature. Order parameter is chosen the strain ε. Rayleigh dissipation is introduced to account for dissipation effect of phase transformation (Bales and Gooding, 1991):

$$F_R = -\frac{1}{2} v \left(\frac{\partial \varepsilon}{\partial t} \right)^2. \tag{3}$$

Here v is the dissipation constant of the material. The dissipation term stands for internal friction due to the movement of interphases (Wang and Melnik, 2012).

It is regarded as a phase transformation viscous effect at the macro-scale.

To derive the governing equation for the SMA wire, the potential energy function is substituted into the Lagrangian function defined in Equation (1), and using Hamilton's principle, the dynamic of the mechanical field could be described by the governing equation as follows:

$$\rho\ddot{u} = \frac{\partial}{dx}\left[k_1(\theta-\theta_c)\varepsilon + k_2\varepsilon^3 + k_3\varepsilon^5\right] + \frac{\partial}{\partial t}\frac{\partial^2 u}{\partial x^2}. \quad (4)$$

The above equation could be easily re-cast into differential-algebraic equations:

$$\rho\ddot{u} = \frac{\partial\sigma}{dx} + \frac{\partial}{\partial t}\frac{\partial^2 u}{\partial x^2},$$

$$\sigma = \left[k_1(\theta-\theta_c)\varepsilon + k_2\varepsilon^3 + k_3\varepsilon^5\right]. \quad (5)$$

These equations could be used for analyzing the nonlinear dynamics of the SMA rod stimulated by mechanical loadings, with hysteretic behavior captured (Wang and Melnik, 2012).

In the current work, a rod bearing torsional loading is considered. Thus, the order parameter has been substituted by the angular displacement instead of uniaxial displacement *u*. Correspondingly, the constitutive relations of the SMAs is obtained as follows:

$$\tau = k_1(\theta-\theta_c)\gamma + k_2\gamma^3 + k_3\gamma^5, \quad (6)$$

where k_1, k_2, and k_3 are constant; and γ is torsional deformation; and τ is the torque. θ is the material temperature, and θ_c is the critical temperature. It is worthy to note that, materials constant, k_1, k_2, and k_3 have the same meaning and mathematical role as those in Equations (2) and (6), but their values should be completely different since is used for modeling different deformation.

Modeling of SMA spring dynamics

In the previous section, the constitutive relation of a rod is given under the circumstance of torsional deformation. Assuming that the rod can be treated as wire, and when the wire is winded up into a coil, it forms the SMA spring. The design of SMA spring shares many similarities with the conventional one (Wahl, 1963). The basic design standard can be found in most mechanical design books, and it is outlined below for the convenience of discussion.

It is assumed in the SMA spring and wire that, the shear strain varies linearly with the radial location for a given angular deflection. The γ (shear strain) is termed as a function of the φ (angular deflection), and r is the radial location, as shown in Figure 2:

$$\gamma(r) = \frac{\varphi r}{L}, \quad L = (\pi Dn/\cos\beta), \quad (7)$$

where L is wire active length of helical spring with β as helix lead angle, which is 5° for close-coiled. And n and D stand for a number of turns and diameter of the SMA spring, respectively. Since $\cos\beta$ is very close to unity, here L can be approximated as:

$$L = \pi nD, \quad (8)$$

where n and D stand for a number of turns and diameter of the SMA spring, respectively.

When the spring was made, an external load is applied as shown in Figure 1. The displacement or deformation x shares the following relationship with

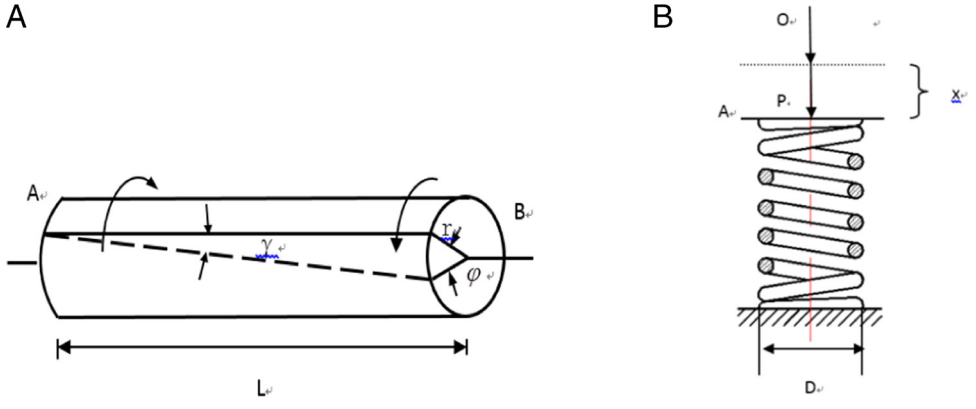

Figure 1: (A) SMA rod under torsion; (B) SMA spring under deformation.

φ, which is the angular spring wire with reference to the other:

$$x = \frac{\varphi D}{2}. \tag{9}$$

The active wire length corresponds to the rod length in Figure 1. The SMA helical spring analysis reduces to pure torsion of a straight wire using the above assumption. Then whenever the SMA spring reaches its equilibrium state, it is controlled by the two forces, resisting the torsional moment and *F*. Therefore, the torque *T* equals:

$$T = \frac{FD}{2}. \tag{10}$$

The torque that the spring wire bears can also be calculated by integrating the shear stress over the radial location as:

$$T = \int_0^r \left(2\tau\pi r^2\right). \tag{11}$$

Since the relation between a straight SMA wire and an SMA spring is obtained, the constitutive relation of the spring can be derived by substituting the above relations into Equation (6), which will give the following force versus displacement relationship:

$$F = \frac{k_1\left(\theta - \theta_c\right)r^4}{4R^3 n}x + \frac{k_2 r^6}{24\pi^2 R^7 n^3}x^3 + \frac{k_3 r^8}{128\pi^5 R^{11} n^5}x^5. \tag{12}$$

This can be reduced to the following equation for the convenience of discussion:

$$F = A_1\left(\theta - \theta_c\right)x + A_2 x^3 + A_3 x^5. \tag{13}$$

To model the dynamic response of SMA spring, the time-independent Ginzburg–Landau theory is used and is formulated using the Helmholtz free-energy equation as follow:

$$\frac{dx}{dt} = -\mu\frac{\partial\psi\left(x\right)}{\partial x} + \Gamma, \tag{14}$$

where μ stands for coefficient of dissipation effects in the phase transformation process and Γ stands for the external input to the system. The input is the mechanical field *F*, so the SMA spring dynamic process of loading–unloading can be expressed as:

$$\xi\frac{dx}{dt} = A_1\left(\theta - \theta_c\right)x + A_2 x^3 + A_3 x^5 - F, \tag{15}$$

where $\xi = -1/\mu$ can be seen as the time constant in the current differential equation. If the loading force *F* is very slow or kept as a constant, the system will get to an equilibrium state when this is set (setting $(dx/dt) = 0$):

$$F = A_1\left(\theta - \theta_c\right)x + A_2 x^3 + A_3 x^5. \tag{16}$$

From Newton's third law, by comparing Equations (16) and (13), the input force to the system equals the restoring force itself. It is observed that hysteresis is wrapped in Equation (15), as shown by the *F-x* relation sketched in Figure 2. As the load of the SMA spring reached a certain value, it will jump to the stable part of the curve CD. Similarly, when the spring

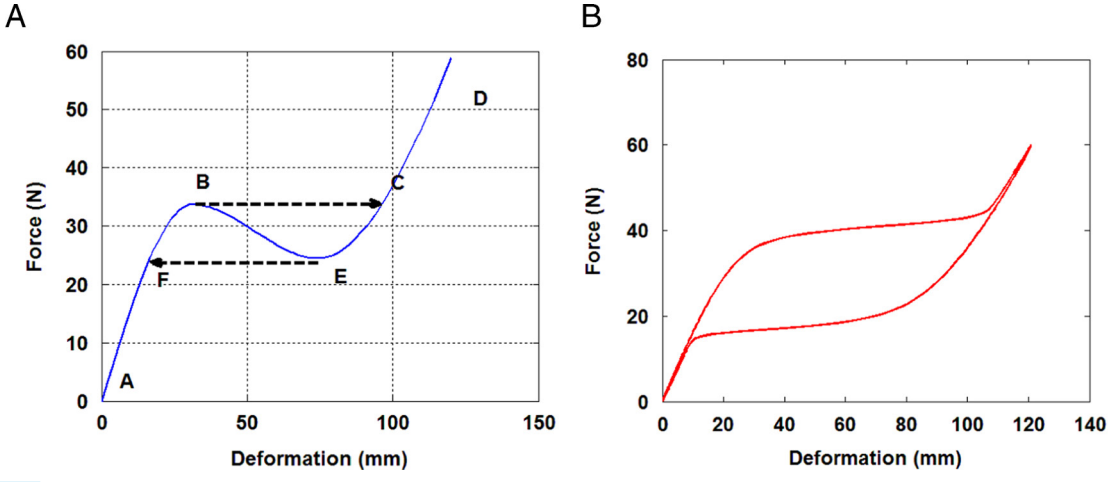

Figure 2: (A) Recovery force of SMA spring; (B) observed hysteresis in simulation results.

is unloaded to point E, it will come instantaneously to the curve FA. This yields the hysteresis behavior, and this hysteretic behavior is caused by the phase transformation induced in the SMA material and is mimicked by the bifurcation of the non-convex dynamics of the SMA spring model.

According to the test data of strong nonlinear SMA spring (Savi et al., 2015), a mechanical field $30 \times \cos(2 \times pi \times f \times t)$ is exerted on the current differential model, and the actual hysteresis is observed in (b). It means that when the system is under the dynamic process of loading–unloading, it will show the inherent hysteresis phenomenon. This indicates that the differential model constructed above can perfectly capture the pseudoelastic character of SMA spring. The recovery force can be easily obtained hence it is applicable in the engineering aspects.

Experimental procedure

In order to verify the proposed model, a series of experimental tests are performed on a testing system design specifically for the purpose. SMA Nitinol wire with 1.5 mm diameter was used for this research. The wire was winded up around a steel shaft with diameter 16 mm and made into an SMA spring. Then it was put in a furnace and heated up to 500°C, annealed for 30 to 40 mins, then cooled in air. The critical temperature θ_c was set to be 35°C (Wang and Melnik, 2012). Six active coils were cut and hooked at both ends and inserted into a hot water chamber designed for this purpose. The chamber has a digital thermometer and thermostat, with a regulatory temperature switch. The chamber was mounted on a universal tension machine for data acquisition. The experimental set up is shown in Figure 3.

A series of experiments concerning the pseudoelasticity of SMA under different constant temperatures were performed (Aguiar et al., 2010). The produced SMA spring is with an initial length of 10 mm. The SMA spring was extended using a constant working frequency, which means, the strain rate of SMA spring was constant during the deformation (Ma et al., 2013). In the current investigation, the experiment focus is on the influence of temperature on the SMA's pseudoelasticity. Experiments at different temperatures above the phase transformation temperature (35°C) were performed. Those experimental

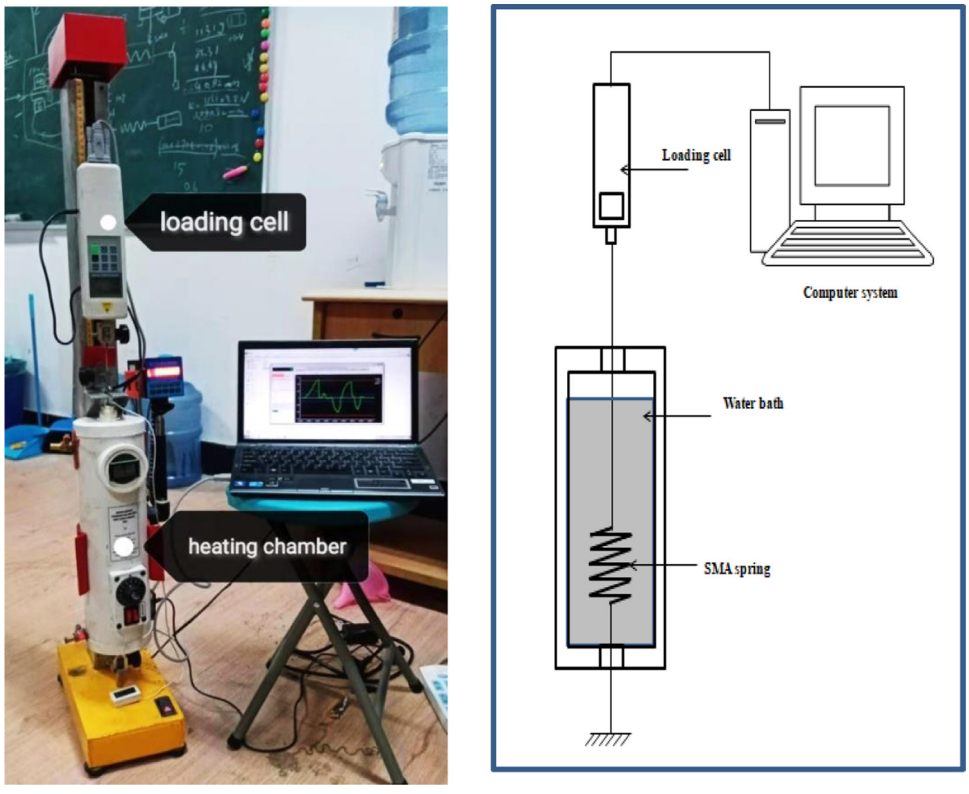

Figure 3: The experimental setup for testing SMA spring.

data obtained at temperature 50°C, 70°C, and 90°C are chosen for the following discussion since it is representative, and will be presented together with its numerical counterparts for comparison purpose.

Result and discussion

To obtain the pseudoelasticity of single-crystalline SMA spring at first, the heating chamber was heated to (50°C, 70°C, and 90°C) which are above the critical austenite-martensite phase transformation temperature 308K (35°C) of the SMA spring sample. The spring was then extended to the length of 85 mm at a constant speed on the tension test machine and then reverted back to zero position at the same speed at each of the above temperature. The corresponding tracked force–deformation values were recorded in a computer through a loading cell as shown in Figure 4A. For the convenience of simulation and comparison, the deformation of SMA spring is rescaled by dividing with 100 in order to make its absolute value less than 1.

From the experimental curve, it is illustrated clearly that, when the temperature is above the critical values and not very high, the pseudoelasticity of the SMA spring is obvious and the related hysteresis loop has an approximate horizontal plateau during loading and unloading process, which could be easily explained by martensite-austenite phase transformation induced in the SMA spring. Whilst with the same loading profile, but at much higher temperature at 90°C, the hysteresis loop still occurs, but there is no horizontal plateau that exists during the loading and unloading process. This fact could be explained by the theory that, at high temperature, the coupled thermoelastic property of the SMA spring is more pronounced, and the influence of martensite-austenite phase transition becomes more and more minor.

Simulation of SMA spring

By using the proposed SMA spring model given in Equation (16), there are five model parameters, which are ξ, θ_c, A_1, A_2, A_3, need to be identified. F is the applied driving force; x is the displacement or deformation of the SMA spring. Using Equation (15):

$$\xi \frac{dx}{dt} + A_1(\theta - \theta_c)x + A_2 x^3 + A_3 x^5 = F,$$

The parameter identification strategy is to tune the model parameter values, thus to fit numerical hysteresis loops to the experimental counterpart as close as possible, which is actually a least square approximation problem in mathematics:

$$\min_{A_1,A_2,A_3,A_4,A_5} G = \sum_{i=1}^{n} \left(\tilde{C}_i - C_i \right)^2, \qquad (17)$$

where n is the number of sampling points; $\tilde{C}_i$ is the experimental data; and C_i is the numerical simulation counterpart. For the convenience of simulation and comparison, the deformation of SMA spring is rescaled by dividing with 100 in order to make its absolute value less than 1.

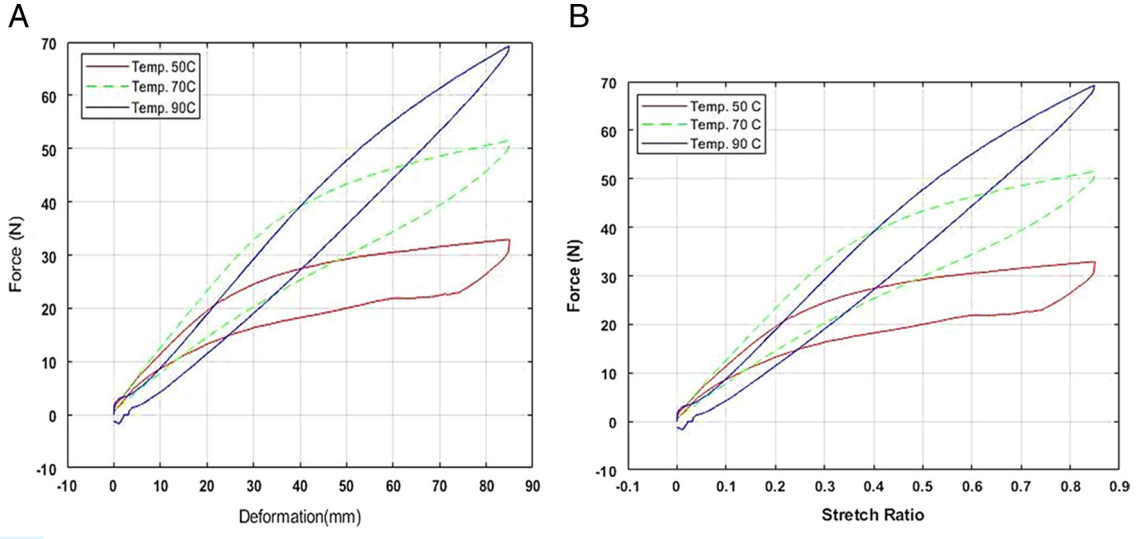

Figure 4: Loadings and unloading at different temperatures and constant loading rate (A) before rescaling; (B) after rescaling.

By applying the above mentioned model parameter identification strategy, the model parameters after rescaling can be determined as: $\xi = 803\,\text{N.s}$, $A_1 = 0.65\,\text{N/K}$, $A_2 = -56.5\,\text{N}$, $A_3 = 31.7\,\text{N}$, $\theta_c = 223.6\,\text{K}$. Using the SMA spring parameters identified above, the simulated force–deformation relation for SMA spring at 323 K (50°C) is simulated and compared with the experimental data. The applied forces are 32.9, 51.5, and 69.2 N for the three simulations done. For the clarification purpose, the simulated and experimental curves are plotted in the same figure, as shown in Figure 5.

It is shown clearly that the simulated curve agrees very well with the experimental data, this good fitness indicates that the proposed model could capture the pseudoelastic property of the SMA very well, at least at the chosen temperature and loading profile. But, it is also obvious that the fitness of the numerical curve with its experimental counterpart is not that perfect at the tip end and the origin of the hysteresis loop during the unloading. The discrepancy between can be reasonably attributed to experimental error, or model error, or other ignored factors in the current investigations.

In order to verify the capability of the proposed model for different SMA springs working temperatures, the simulated force-stretch ratio curve for the SMA spring at a constant temperature of 70°C is compared with its experimental data. The model parameters used for the simulation is still the same as those used in the previous comparison. The simulated curve is also plotted together with its experimental counterpart, as shown in Figure 6.

It is shown clearly that, once again, the simulated force–deformation curve captures the hysteresis loop precisely, and agrees very well with the experimental force-stretch ratio curve. Only at the area close to the origin and the tip end, the small difference is observable.

To validate the proposed model with even higher temperature, the simulated force-stretch ratio curve of the SMA spring at a temperature of 90°C is presented with its experimental counterpart again in the same figure, as shown in Figure 7. The agreement between the numerical and experimental curves is even better than those at lower temperatures. The improvement of the fitness of model results to experimental data at higher temperature could be attributed to the fact that, at higher temperature, there is no martensite phase transformation induced, and the dynamics of the SMA spring is just nonlinear thermoelastic dynamics problem, which is much easier to handle compared to those with phase transformation induced.

Via the comparison of the simulated and experimental force-stretch ratio curves at three representative temperature, it could be concluded that the proposed model is capable of capturing the hysteretic dynamics of the SMA spring, no matter there is martensite transformation induced in the material or not. To make the comparison more clear, the simulated and experimental force-Stretch ratio curves of the SMA spring at three different temperatures are all plotted in the same figure, such that the influence of the temperature to the SMA spring is clearer (Figure 8).

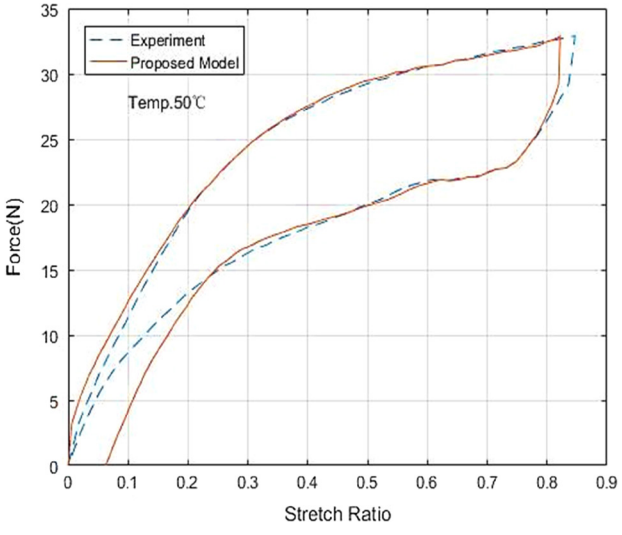

Figure 5: Comparison of numerical and experimental SMA spring responses at 50°C.

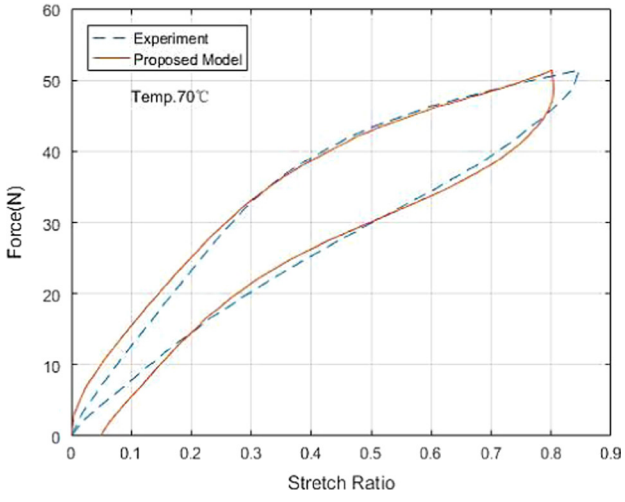

Figure 6: Comparison of numerical and experimental SMA spring responses at (70°C).

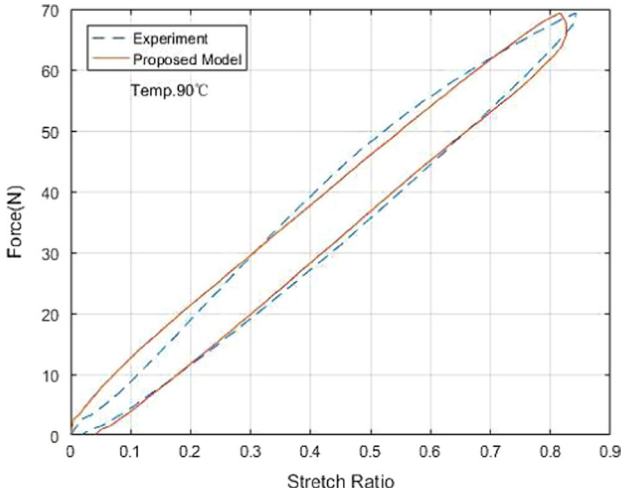

Figure 7: Comparison of numerical and experimental SMA spring responses at 90°C.

It is shown that, as the temperature rises, the hysteresis loop becomes more and more tilted upwards. The same loading force will induce large deformation of the SMA spring at a higher temperature. Theoretical analysis of the SMA spring leads us to expect the following. At lower a temperature (but still higher than the critical temperature), the external force will induce martensite transformation in the SMA spring, therefore, it will behave in a pseudoelastic way. In other words, hysteresis loops should exist in its force-Stretch ratio curve, and there should be a roughly horizontal plateau in the curve during loading and unloading. This expectation is verified by the numerical and experimental results simultaneously. As the temperature is increased, the chances for external forces to induce martensite transformation become less and less, which means phase transformation induced deformation has smaller contributions whilst conventional thermoelastic behavior playing a more and more pronounced role in the force-Stretch ratio curves. This analysis is also verified by the experimental and numerical hysteresis loop at a temperature of 70°C, which is tilted upward compared to the one at 50°C, the plateau in the loops becomes less noticeable. It is also expected that, at an even higher temperature, there will be no martensite transformation and the SMA spring will become a conventional thermoelastic spring, but with internal friction. The numerical and experimental results verified this expectation firmly and clearly, as illustrated in the figure. At 90°C, the SMA spring behaves very regularly, except the hysteresis loop still exist in the force-Stretch ratio curve, which could be attributed to the internal friction property of the SMA property and other friction effects.

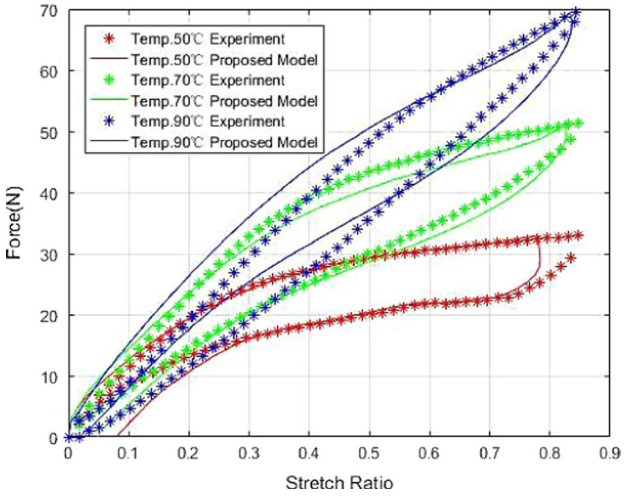

Figure 8: Comparison of numerical and experimental SMA spring responses.

Conclusion

In this paper, a one-dimensional single-crystalline constitutive model for SMA spring is constructed based on the Ginzburg–Landau theory by combining the theory of mechanical spring and the derived SMA rod constitutive relation. Simulations and experimental tests are performed, numerical results are compared with their experimental counterpart and very well agreement is achieved. The simulated hysteresis loops agree with the theoretical analysis. The proposed model is formulated as a second-order ordinary differential equation, which is very convenient for system dynamic analysis and implementing of modern control technology. It is therefore easy to see the convenience of the proposed model for engineering applications.

Acknowledgments

This research is sponsored by the National Natural Science Foundation of China (Grant Nos 51575478 and 61571007).

Literature Cited

Aguiar, R. A. A., Savi, M. A. and Pacheco, P. M. C. L. 2010. Experimental and numerical investigations of shape memory alloy helical springs. *Smart Materials and Structures* 19(025008): 9.

Alahi, E. E., Nag, A., Chandra, S. and Burkitt, L. 2018. Sensors and actuators A: physical A temperature-compensated graphene sensor for nitrate monitoring in real-time application. *Sensors and Actuators A: Physical* 269: 79–90.

Bales, G. S. and Gooding, R. J. 1991. Interfacial dynamics at a first-order phase transition involving strain. *Physical Review Letters* 67(24): 3412–3415.

Dong, Y., Boming, Z. and Jun, L. 2008. A changeable aerofoil actuated by shape memory alloy springs. *Materials Science and Engineering A* 485(1–2): 243–250.

Enemark, S., Santos, I. F. and Savi, M. A. 2016. Modelling, characterisation and uncertainties of stabilised pseudoelastic shape memory alloy helical springs. *Journal of Intelligent Material Systems and Structures* 27(20): 2721–2743.

Gédouin, P., Pino, L., Arbab, S., Calloch, S., Delaleau, E. and Bourgeot, J. 2019. Sensors and actuators A: physical R-phase shape memory alloy helical spring based actuators: modeling and experiments. *Sensors and Actuators A: Physical* 289: 65–76.

Kumar, P. K. and Lagoudas, D. C. 2008. Introduction to shape memory alloys.

Liang, C. and Rogers, C. A. 1990. One-dimensional thermomechanical constitutive relations for shape memory materials. *Journal of Intelligent Material Systems and Structures* 1(2): 207–234.

Liang, C. and Rogers, C. A. 1993. Design of shape memory alloy springs with applications in vibration control. *Journal of Vibration and Acoustics* 115(1): 129–135.

Ma, J., Huang, H. and Huang, J. 2013. Characteristics analysis and testing of SMA spring actuator. *Advances in Material Science and Engineering* 2013(1): 1–7.

Morin, C., Moumni, Z. and Zaki, W. 2011. A constitutive model for shape memory alloys accounting for thermomechanical coupling. *International Journal of Plasticity* 27(5): 748–767.

Pirbhulal, S. 2019. Medical information security for wearable body sensor networks in smart healthcare. *IEEE Consumer Electronics Magazine* 8(5): 37–41.

Pirbhulal, S., Zhang, H., Alahi, E. E. and Ghayvat, H. 2017. A novel secure IoT-based smart home automation. *Sensors* 17(69): 1–19.

Rao, A., Srinivasa, A. R. and Reddy, J. N. 2015. Design of shape memory alloy (SMA) actuators.

Savi, M. A., Pacheco, P. M. C. L. and Garcia, M. S. 2015. Nonlinear geometric influence on the mechanical behavior of shape memory alloy helical springs 24: 035012.

Tobushi, H. and Kikuaki, T. 1991. Deformation of a shape memory alloy helical Spring. *SME International Journal* 34(1): 83–89.

Toi, Y., Lee, J. and Taya, M. 2004. Finite element analysis of superelastic, large deformation behavior of shape memory alloy helical springs. *Materials Science and Engineering A* 82(20–21): 1685–1693.

Wahl, A. M. 1963. *Wahl, A. M. Mechanical Springs*, McGraw-Hill, London.

Wang, J., Moumni, Z. and Zhang, W. 2017. A thermomechanically coupled finite-strain constitutive model for cyclic pseudoelasticity of polycrystalline shape memory alloys. *International Journal of Plasticity* 97: 194–221.

Wang, L. and Melnik, R. V. N. 2012. Nonlinear dynamics of shape memory alloy oscillators in tuning structural vibration frequencies. *Mechatronics* 22(8): 1085–1096.

Wang, L. and Melnik, R. V. N. 2004. Dynamics of shape memory alloys patches. *Materials Science and Engineering A* 378(1–2): 470–474.

Wu, W., Pirbhulal, S. and Kumar, A. 2018. Optimization of signal quality over comfortability of textile electrodes for ECG monitoring in fog computing based medical applications optimization of signal quality over comfortability of textile electrodes for ECG monitoring in fog computing based medical applications. *Future Generation Computer Systems* 86(January): 515–526.

Zhou, C., Wang, L. and Feng, C. 2009. Nonlinear differential equation approach for the two-way shape memory effects of one-dimensional shape memory alloy structures. *The International Society for Optical Engineering*, pp. 12–14.

Appendix

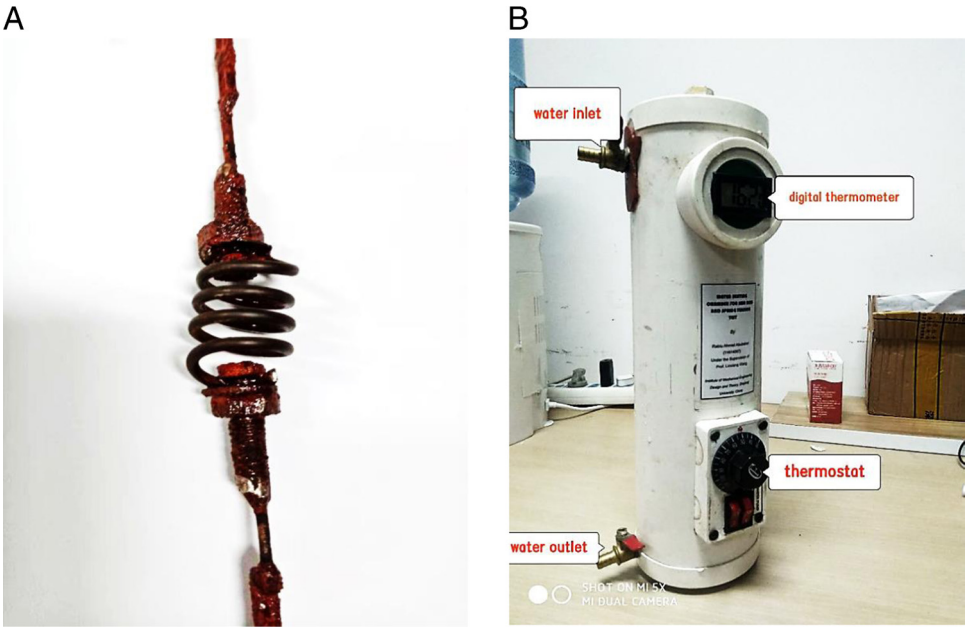

Figure A1: (A) the SMA spring sample; (B) the SMA spring heating chamber.